Composite Energy Storage System Involving Battery and Ultracapacitor With Dynamic Energy Management in Microgrid Applications

Haihua Zhou, *Student Member, IEEE*, Tanmoy Bhattacharya, Duong Tran, Tuck Sing Terence Siew, and Ashwin M. Khambadkone, *Senior Member, IEEE*

***Abstract*—Renewable-energy-based microgrids are a better way of utilizing renewable power and reduce the usage of fossil fuels. Usage of energy storage becomes mandatory when such microgrids are used to supply quality power to the loads. Microgrids have two modes of operation, namely, grid-connected and islanding modes. During islanding mode, the main responsibility of the storage is to perform energy balance. During grid-connected mode, the goal is to prevent propagation of the renewable source intermittency and load fluctuations to the grid. Energy storage of a single type cannot perform all these jobs efficiently in a renewable powered microgrid. The intermittent nature of renewable energy sources like photovoltaic (PV) demands usage of storage with high energy density. At the same time, quick fluctuation of load demands storage with high power density. This paper proposes a composite energy storage system (CESS) that contains both high energy density storage battery and high power density storage ultracapacitor to meet the aforementioned requirements. The proposed power converter configuration and the energy management scheme can actively distribute the power demand among the different energy storages. Results are presented to show the feasibility of the proposed scheme.**

***Index Terms*—Bidirectional converter, energy management, energy storage, interleaved modulation, modular design and microgrid.**

I. Introduction

DUE to the intermittent nature of renewable energy sources and the continuous variations of the load, storage (e.g., battery, ultracapacitor, flywheel etc.) is usually needed in a renewable powered microgrid. The renewable output power profile and the load profile are two important factors in deciding the capacity and type of the energy storage components. The variation in output power from a utility-scale PV system is presented in [1], which is shown as curve (a) in Fig. 1, whereas curve (b) of Fig. 1 depicts a typical load profile. Both the PV power and load power profiles are normalized such that they have equal average power. The PV power output profile and the load profile shows low-frequency as well as high-frequency fluctuations, which are mutually independent in nature. Hourly average variations can be considered as low-frequency variation, whereas power transients, which sustain for minutes, seconds, or milliseconds come under the high-frequency segment. To buffer out the low-frequency oscillations and to compensate for the intermittency of the renewable energy sources, energy storage with high energy density is required. To provide high-frequency component of power and also to supply or absorb the high-power transients, energy storage with high power density is required. Fig. 2 shows the energy density and power density profiles of different energy storages, whereas a general theory of Ragone plot is provided in [2]. It is to be noted that, the load profile and renewable source profile strictly decides the desired location of the optimum energy storage on the Ragone chart and this location will be different for different microgrids. If we use only battery as storage, then it has to be oversized to take care of the peak load demand. If we use only ultracapacitor, then it has to be oversized for storing large amount of energy to take care of the intermittency of the renewable sources and loads.

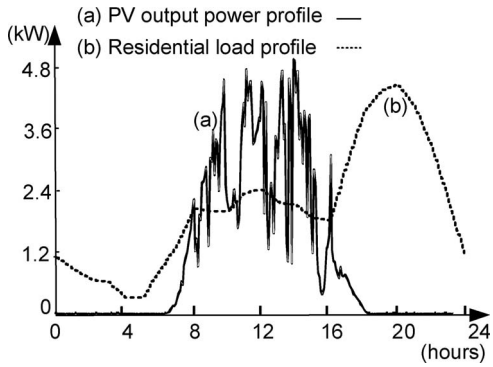

Fig. 1. Typical 24-h (a) PV output power and (b) residential load profile.

Hence, use of a Composite energy storage system (CESS) comprising both high power density and high energy density storage units is practically unavoidable. Now, the selection of the type of storage is also crucial. For energy storage in the high power range for standard power systems, the most suitable ones would be pumped hydro storage, compressed air storage, etc.

Manuscript received July 5, 2010; revised November 3, 2010; accepted November 8, 2010. Date of current version May 13, 2011. The work was supported by the Science And Engineering Research Council (SERC) under MODERN project Fund R-263-000-507-305. Recommended for publication by Associate Editor J. M. Guerrero.

H. Zhou, T. Bhattacharya, D. Tran, and T. S. T. Siew are with the Department of Electrical and Computer Engineering, National University of Singapore, Engineering drive-3, Singapore 117576 (e-mail: g0500090@nus.edu.sg; eletb@nus.edu.sg; g0700253@nus.edu.sg; terence_siew@nus.edu.sg).

A. M. Khambadkone is with the Department of Electrical and Computer Engineering, National University of Singapore, Engineering drive-3, Singapore 117576, and also with the Experimental Power Grid Center, Agency for Science, Technology and Research (A*STAR), Singapore 138668 (e-mail: ashwinmk@ices.a-star.edu.sg).

Digital Object Identifier 10.1109/TPEL.2010.2095040

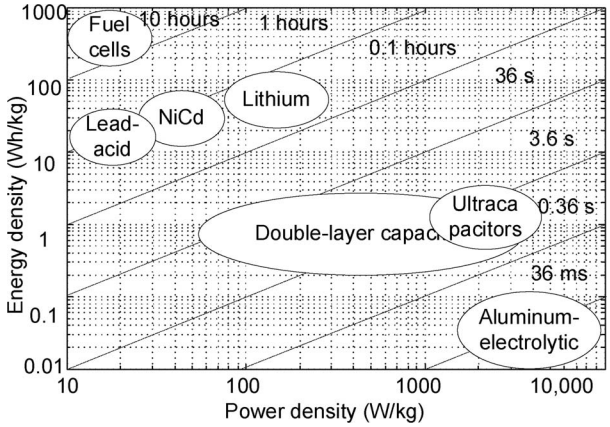

Fig. 2. Ragone chart showing the power density and energy density of different storages.

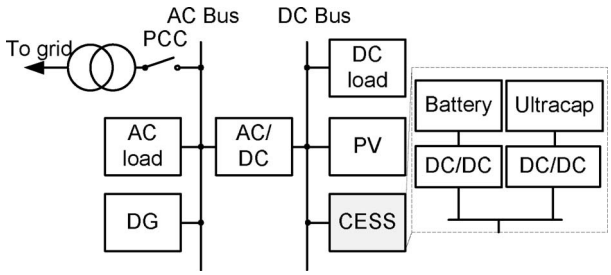

Fig. 3. Block diagram showing CESS interface with the dc grid.

However, for microgrids, where power levels are in the range of a few megawatts, battery, ultracapacitor, and flywheel are the more suitable options. Battery and ultracapacitor are considered as high energy density storage and high power density storage, respectively, and their combination is a very promising option to realize the CESS system. Glavin *et al.* [3] shown that ultracapacitor–battery hybrid energy storage performs better than battery-alone energy storage for a stand-alone PV system. Guoju *et al.* [4] shown that battery–ultracapacitor hybrid storage has the virtues of both high energy density and high power density, and also, such system increases battery life. Dougal *et al.* [5] analytically proved that battery–ultracapacitor hybrid achieves power and life extension of battery. This paper also exploits the potential of battery and ultracapacitor as a CESS, as shown in Fig. 3.

Bidirectional dc–dc converters are required to interface the battery banks and the ultracapacitor to the dc link for controlling the power flow. The basic requirement from the dc–dc converter is that the user should be able to dynamically allocate the load current demand between the battery and the ultracapacitor. Different power converter structures are proposed in the literature for interfacing battery and ultracapacitor to the dc link. Niemoeller and Krein [6] proposed that an ultracapacitor with a boost chopper can be connected to the terminals of the battery, and battery current can be indirectly controlled by controlling the ultracapacitor current. Guidi *et al.* [7] proposed a technique, where ultracapacitor is connected to the battery with reduced power device rating. Both the schemes have the problem that if it is used for microgrid application, many batteries have to be connected in series to form a high-voltage dc link resulting in reduction of volumetric efficiency of the battery bank. One of the scheme proposed in [8] talks about using two individual dc–dc choppers, one each for battery bank and ultracapacitor, for interfacing them to the dc link. Garcia *et al.* [9] used bidirectional boost converters for interfacing both ultracapacitor and battery to the dc link. However, none of the aforementioned topologies talk about the scenario when large number of battery banks need to be interfaced to the dc link to meet the power and energy demands of a microgrid. To achieve high power and high flexibility, modular design is the best approach [10]–[12]. The modular power converter structure proposed in [13] by Zhou *et al.* provides the flexibility of interfacing multiple battery banks and ultracapacitor to the dc link. The structure is so modular that power and energy rating of the CESS can be scaled up to any level independently.

For the modular power converter structure, any bidirectional isolated dc–dc converter can be used as a single module. Phase-shift-controlled dual active bridge (DAB) converter [14]–[16] is a promising configuration for modular power converter synthesis. It is able to transfer power bidirectionally just by adjusting the phase shift between the primary- and secondary-side bridges. The isolation between energy storage and load is fulfilled by high-frequency transformer. As soft switching of DAB is possible, high switching frequency operation can be achieved, even at high power levels, and hence, the size of filter capacitors and isolation transformers can be drastically reduced. Therefore, DAB is selected as basic module in the proposed scheme.

A proper energy management scheme is required to extract the benefits of the proposed CESS. Garcia *et al.* [9] divides the power demand into low-frequency and high-frequency components. The converter current references are set such that low-frequency components are supplied by the battery and the high-frequency components are supplied by the ultracapacitor. Li and Joos [8] also adopted a similar approach. Garcia *et al.* [9] proposed a closed-loop ultracapacitor voltage-control scheme too. However, these aforementioned control strategies are practical when only one battery bank and one ultracapacitor are used as the hybrid energy storage. When multiple battery banks and ultracapacitor are used, then a proper energy management scheme, which can take care of charge balancing among battery banks, online battery replacement, etc., along with the functions performed in [8] and [9], is required. An initial step toward such energy management scheme is proposed in [13].

Hence, this paper proposes a CESS using modular interleaved bidirectional DAB converter to satisfy the different needs in the microgrid. A new modular power converter configuration for interfacing batteries and ultracapacitor to the dc link is proposed. In order to regulate the output voltage and to achieve flexible power distribution among modules, a cascaded control loop comprising inner current-control loop and outer voltage-control loop is incorporated. The salient features of the proposed CESS system are: 1) dynamic allocation of steady power demands and transient power demands to the batteries and ultracapacitor, respectively; 2) flexible distribution of power flow among different batteries without disturbing the normal operation and online bat-

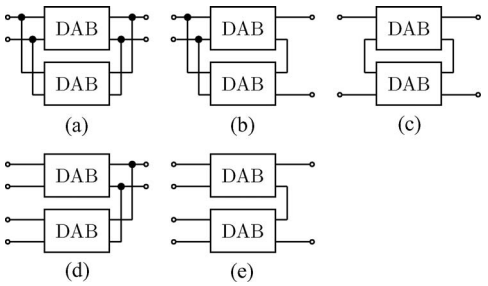

Fig. 4. Few possible configurations of module-based converter. (a) IPOP. (b) IPOS. (c) ISOS. (d) Modified version of IPOP. (e) Modified version of IPOS.

tery replacement; (3) ultracapacitor charging–discharging without disturbing the normal operation; and (4) flexibility to upgrade the power rating or energy rating of the CESS system independently. Incorporation of these features has been possible because of the proposed unique modular power converter structure.

This paper is structured as follows. Section II explains the advantages of modular power converter design approach. Section III explains the proposed modular power converter structure for interfacing batteries and ultracapacitors to the dc link. The control strategy of DAB modules for energy management of the CESS system is explained in Section IV. Experimental results from a laboratory prototype of the proposed system are presented in Section V. Finally, the paper is concluded in Section VI.

II. Family of Modular Converters

As mentioned earlier, module-based design is the best approach to satisfy all the requirements of energy storage and load. The configurations of module-based converter are shown in Fig. 4. Input parallel output parallel (IPOP) configuration, as shown in Fig. 4(a), shares the input and output current in modules. By controlling the input current in each of the converters, the power flow in each can be controlled [17]. Fig. 4(d) is derived from Fig. 4(a) to interface multiple sources. This is also a common topology in connecting multiple sources [18]. Input parallel output series (IPOS) topology presented in Fig. 4(b) shares the current in the parallel side, while achieves high voltage in the series side. Therefore, it is suitable for applications, where energy storage and load have large voltage difference. Fig. 4(e) is derived from Fig. 4(b) to interface multiple sources. Input series output series (ISOS) configuration of Fig. 4(c) shares voltage both in input and output side. It is favorable for high input and output voltage application. This connection is especially useful when power increases to megawatt level, since higher voltage can help to reduce the magnitude of current to achieve lower loss [12], [14]. In all the aforementioned schemes, the basic power converter module used is the DAB, as shown in [14]–[16]. The module-based converter design approaches not only can match the different source and load requirements, but also share the power in each module, and thus help to reduce the switch stress. Table. I lists the comparison of switch stress and transformer turns ratio in IPOP, IPOS, and ISOS with single DAB converter, respectively. Base values are chosen according to single DAB rating when same power and same input/output voltage are used. From Table. I, we can clearly see the advantages of different topologies in switch rating selection. For example, the current rating for primary-side switches and voltage rating for the secondary-side switches are reduced to $1/n$ p.u. (as shaded rows) when n modules are connected under IPOS structure.

TABLE I
Comparison of Device Stress Under Same Output Power

	IPOP (p.u.)	IPOS (p.u.)	ISOS (p.u.)
Primary			
Switch Current Rating	$1/n$	$1/n$	1
Switch Voltage Rating	1	1	$1/n$
Secondary			
Switch Current Rating	$1/n$	1	1
Switch Voltage Rating	1	$1/n$	$1/n$
Turns ratio	1	$1/n$	1

This modular design approach is followed in realizing the power converter structure in the proposed CESS system.

III. Proposed Power Converter Structure

As shown in Fig. 3, the CESS system consists of both high energy density and high power density storage. Battery is selected here as a high energy density storage. Due to intermittent nature of the renewable energy sources, the battery needs to source or sink energy for a long period of time. Therefore, battery capacity has to be high, which can be achieved by connecting multiple battery banks. Connecting too many batteries in series reduces the volumetric efficiency of the battery bank. For interfacing ultracapacitor with dc bus, one has to consider that the terminal voltage of ultracapacitor is less (around 28–45 V), while the dc bus is regulated at high voltage (around 800 V for connecting an inverter interfacing a 415-V 3-phase 4-wire system). The ultracapacitor needs to supply or absorb high current for a short duration of time. Considering these requirements, the modular power converter structure adopted for interfacing battery and ultracapacitor to the dc bus is shown in Fig. 5. The added advantage of such modular structure is that if n parallel DAB branches are used, then by applying the interleaving scheme, the input-current and output-voltage ripple frequency can be increased by a factor of n and ripple magnitude can be reduced to less than $1/n$ compared to single DAB. At this point, it is important to explore the reconfigurability of the proposed modular power converter structure of Fig. 5. If the energy density of the CESS needs to be increased, then we can add parallel branches to the battery side, as shown in Fig. 5. High energy density may be required, if the microgrid is powered from only renewable sources. Similar way, more ultracapacitor branches can be added to increase the power density of CESS. High power density may be required for CESS used in traction application, where high burst of power is supplied or absorbed during acceleration or braking, respectively. Moreover, the power converter structure can be easily reconfigured to achieve different dc-link voltage levels, as shown in Fig. 6

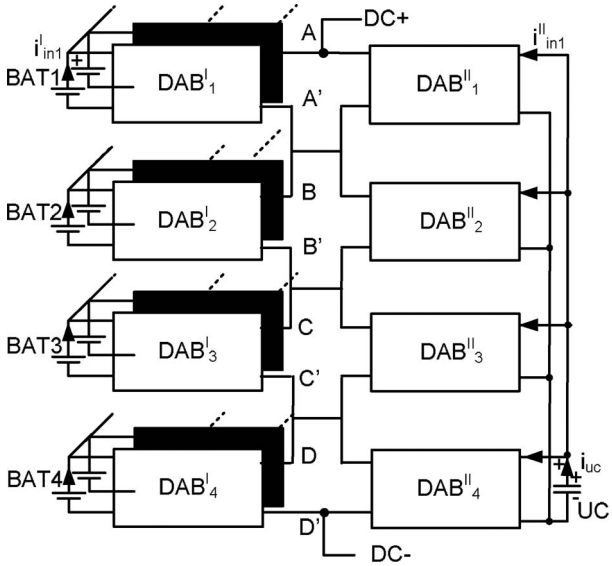

Fig. 5. Topology of the proposed interleaved DAB-based CESS.

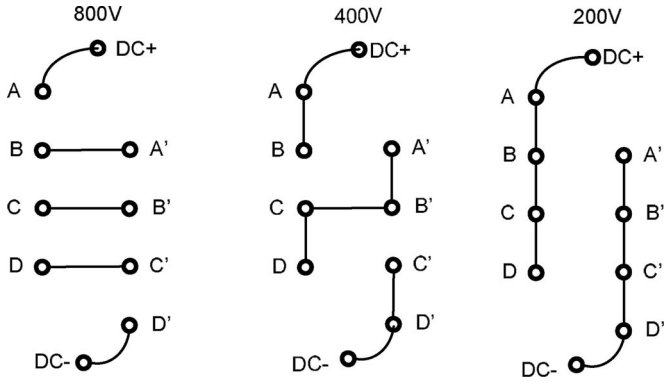

Fig. 6. Reconfiguration of the power converter structure to satisfy different dc-link voltage requirements.

IV. Proposed Control Strategy of DABs for Energy Management of the CESS System

The control scheme for energy management of this CESS system is shown in Fig. 7. The symbols used to represent different variables are defined in the Appendix.

As mentioned in Section I, DAB converter is selected as a basic cell in our application. The power transfer is achieved by phase shifting the voltage across the primary and secondary sides of the high-frequency transformer. The detailed operating principles of DAB is explained in [16]. Every DAB has a current-control loop associated with it. The output of the current controller generates the phase-shift information between the input and output bridges of the DAB module. The task of the energy management block of CESS is to generate appropriate current reference for each DAB module. Three specific cases of power management are discussed in Section IV-A– C. For the analysis, the direction of current flowing out of battery and ultracapacitor is taken as positive, as shown in Fig. 5.

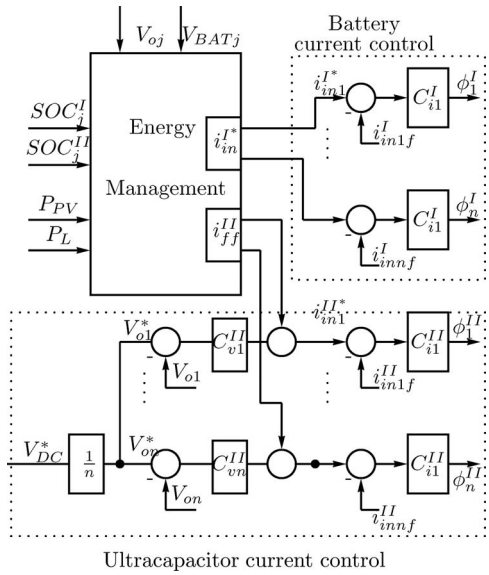

Fig. 7. Control block diagram for the IPOS interleaved DAB converter.

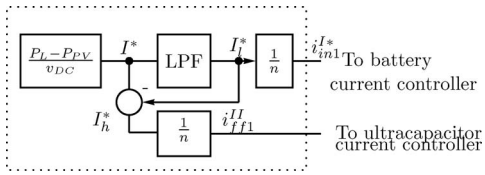

Fig. 8. Energy management strategy for case I.

A. Case I: Dynamic Allocation of Power Demand to Batteries and Ultracapacitor

One objective of the energy management system is to allocate steady power demand to the batteries and transient power demand to the ultracapacitor. We can think of a specific example of a dc grid, where PV generator and load are connected along with the CESS system. The block diagram of the overall control scheme is shown in Fig. 7, and the current reference generation strategy for this specific case is shown in Fig. 8. The total current demand from the CESS system is calculated depending on the difference between energy source power and load power. Here, the current demand can be positive or negative depending on the difference. Then, this current reference is passed through a low-pass filter (LPF) to get the low-frequency component of the current demand. This low-frequency component I^*_l is used to generate the total current reference for the battery interfacing power converters. As there are n parallel DAB branches, the current reference for each branch would be I^*_l/n . In this case, it is assumed that, all the batteries are at the same state of charge (SOC). For controlling the DABs interfacing the ultracapacitor, a cascaded control scheme using inner current-control loop and outer voltage-control loop is realized. The high-frequency component of the current demand from the CESS system is added as feedforward term at the output of the voltage controllers. The value of this feedforward term for each DAB branch is equivalent to I^*_h/n . To verify this control strategy, simulation is carried out in SIMPLORER software.

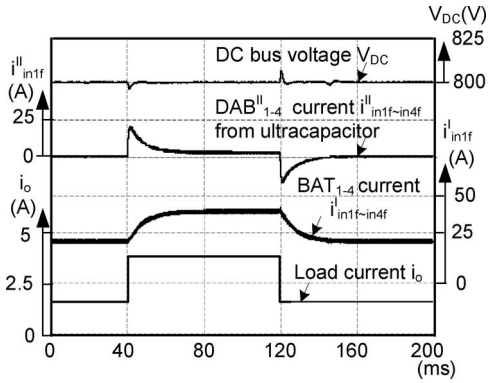

Fig. 9. Dynamic response for a step change in current demand from the CESS system (Case I).

Four parallel branches are considered. Each branch is rated for 1.2 kW. In order to justify the scheme in a practical scenario, up to 20% variation in leakage inductance and output capacitance are considered. Fig. 9 shows the dynamic response of the dc-link voltage and the average converter input currents for step variation in current demand from the CESS system. In practice, a sudden variation in current demand can occur for switching ON or switching OFF some particular load or for sudden change in solar insolation because of passing clouds. At $t = 40$ ms, there is a step increase in the load current. It is evident from Fig. 9 that ultracapacitor-interfacing converter currents $i^{II}_{\mathrm{in}(1f-4f)}$ compensates for the sudden current dynamics, and the battery currents $i^{I}_{\mathrm{in}(1f-4f)}$ slowly increases to cater to the steady load demand. The time constant of the LPF shown in Fig. 8 is kept as only 50 ms to show the operating principle. In practice, this cutoff frequency has to be set depending on the relative capacity of the battery and ultracapacitor. Similar response can be seen for a step decrease in load current at $t = 120$ ms.

B. Case II: Energy Management of the Batteries

In an ideal case, all the batteries can source or sink same current. But in practice, different batteries will be in different states of charge and their equalization is required. In the example of the earlier section, the current reference for all the batteries are set equal as I^*_l/n . However, the energy management scheme can actually allocate different current references for different batteries depending on their states of charge. Fig. 10(a) shows that if same current is drawn from all the four batteries with only one of them having higher SOC, then batteries with lower SOC can go into deep discharge. Hence, if we put a deep discharge limit, then the energy stored in the battery with higher SOC cannot be fully utilized. In fact, this result also indirectly explains that, if many batteries are connected in series to form a high-voltage dc-link, then volumetric efficiency of the battery bank will be decided by the battery with lowest SOC, resulting in reduced energy density. However, if current drawn from individual batteries is proportional to their individual SOCs, then all the batteries will hit the deep discharge limit together and their energy can be fully utilized as shown in Fig. 10(b). In this case, the battery with higher SOC supplies more current till all the batteries reach same SOC. The authors in [19] and [20] explained the needs for SOC control and propose control methods for SOC balancing of the battery units. Guerrero *et al.* [21] emphasized on power sharing among different batteries depending on their charge level and to achieve this, droop coefficient is adjusted to be inversely proportional to their charge level. One extreme case can be a situation when one of the battery current has to be made zero to disconnect it for replacement. Fig. 11 shows the simulation results corresponding to this dynamics. The current reference to the DAB connected to the battery to be replaced is slowly made zero starting at $t = 20$ ms. The reduction of this battery power is compensated by other batteries by increasing their current references. The voltage controllers adjust the current references of the DABs connected to the ultracapacitor to regulate $V_{o(1-4)}$ at the reference value. Fig. 11 shows the dynamic response of the average converter input currents for letting one battery current $i^{I}_{\mathrm{in}1f}$ to become zero. The average currents $i^{I}_{\mathrm{in}(2f-4f)}$ of converters connected to other batteries slowly increase to compensate. Because of this change in battery currents, the input current $i^{II}_{\mathrm{in}1f}$ of DAB^{II}_{1} increases and input currents $i^{II}_{\mathrm{in}(2f-4f)}$ of DAB^{II}_{2-4} decrease to regulate the dc bus.

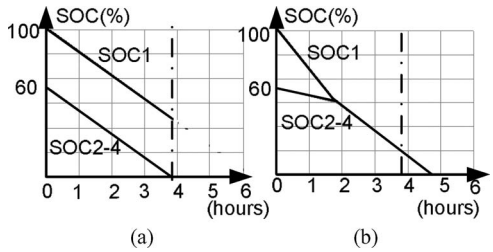

Fig. 10. SOC of all the batteries (a) with equal discharge current and (b) with their discharge current proportional to their SOCs.

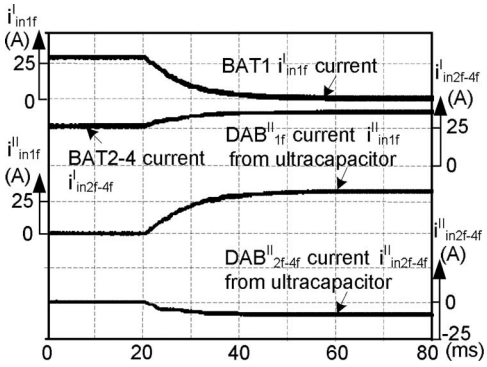

Fig. 11. Dynamic response of converter currents when one battery current reference is made zero (Case II).

C. Case III: State of Charge Control of Ultracapacitor

The ultracapacitor SOC control is also an important requirement of the energy management scheme. The ultracapacitor SOC can be easily estimated from its terminal voltage. The energy management scheme has to maintain the ultracapacitor SOC within a band. If the ultracapacitor voltage falls below the lower band, then the energy management scheme generates appropriate current references for the battery and ultracapacitor.

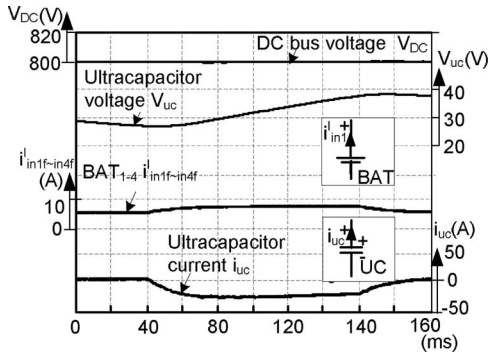

Fig. 12. Ultracapacitor charging scheme (Case III).

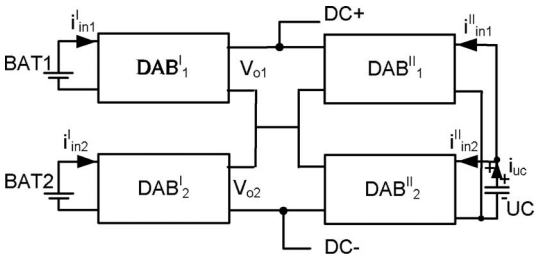

Fig. 13. Block diagram of the experimental setup.

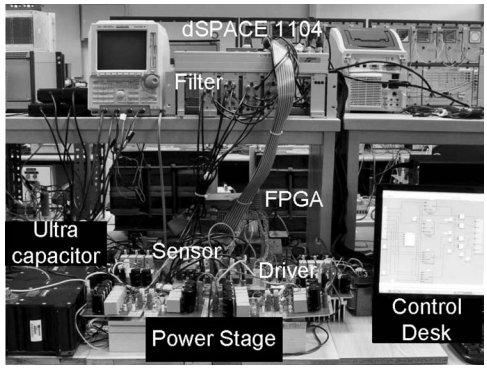

Fig. 14. Experimental setup.

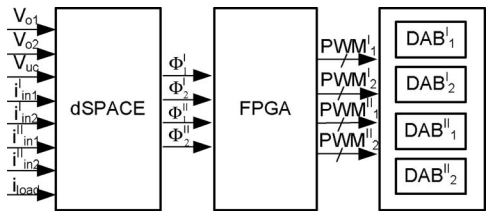

Fig. 15. Block diagram of controller implementation.

The simulation results showing ultracapacitor charging process is presented in Fig. 12. For charging the ultracapacitor, a negative current reference is added to the controllers of the DABs interfacing it to the dc bus. Hence, the ultracapacitor current becomes negative, as shown in Fig. 12. To compensate for this outflow of current from the dc bus, a positive current reference is added to the controllers of the DABs interfacing the batteries to the dc bus. The resulting increase in magnitude of average battery currents $i^{I}_{\mathrm{in}(1f-4f)}$ is shown in Fig. 12. Once the ultracapacitor gets charged, i.e., the ultracapacitor voltage V_{UC} reaches the upper band, this added offset current is removed. Fig. 12 shows that there is no disturbance in the dc-bus voltage V_{dc} throughout this process.

V. Experimental Results

To illustrate the basic principles of proposed energy management controller, two converters interfacing batteries and two converters interfacing ultracapacitors are implemented, as shown in Fig. 13. A picture of the lab prototype is shown in Fig. 14. A low-voltage laboratory prototype is built to prove the concept where nominal battery and ultracapacitor voltages are kept at 24 V, and the total dc-link voltage across the load is rated at 200 V. The controller is implemented in dSPACE 1104 and the gating signals are generated by field-programmable gate array (FPGA) board. The schematic of the experimental controller setup is shown in Fig. 15. Table. II lists all experimental parameters. Similar to the analysis of Section IV, the direction of current flowing out of battery and ultracapacitor is taken as positive.

Fig. 16 is recorded when load steps between 300 and 600 W. As shown in Fig. 16, when step load is applied to the system, the output voltage is well regulated. The current drawn from the BAT1 is slowly increased, while currents from ultracapacitor interfacing converters meet load dynamic response. This verifies the dynamic power-allocation scheme proposed earlier.

Fig. 17 shows the experimental results of the battery shutdown process. To replace BAT1, its power is made zero by bringing down its current to zero. The current drawn from the BAT2 is increased to compensate for the loss of power drawn from BAT1. Currents from two ultracapacitor interfacing converters change accordingly to regulate the dc-link voltage.

Fig. 18 shows the ultracapacitor charging process from the battery. To charge the ultracapacitor from 15 to 20 V, a constant charging current value is added to the battery-current references. The ultracapacitor-interfacing converter currents become negative to regulate the dc-link voltage, and hence, in this process, the ultracapacitor gets charged. Once the ultracapacitor voltage reaches 20 V, the charging current reference is removed and the charging also stops, as seen in Fig. 18.

TABLE II
Experimental Parameters

Rated ultracapacitor voltage (V)	V_{UC}	24
Battery voltage (V)	V_{BAT}	24
Output voltage rating of each DAB (V)	V_{o1}	100
Transformer turns ratio	n	4
Switching frequency (kHz)	f_s	20
Rated output Power of each DAB (W)	P_{o1}	300
Leakage Inductance of DAB^{I}_{1} (μH)	L_{k1}	29.8
Leakage Inductance of DAB^{I}_{2} (μH)	L_{k2}	30.1
Leakage Inductance of DAB^{II}_{1} (μH)	L_{k3}	29.5
Leakage Inductance of DAB^{II}_{2} (μH)	L_{k4}	29.9
Capacitance of output voltage V_{o1} (μF)	C_{o1}	330x3
Capacitance of output voltage V_{o2} (μF)	C_{o1}	330x3

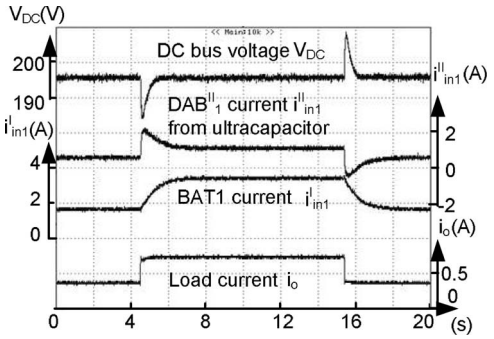

Fig. 16. Experimental result showing dynamic response when load power steps between 300 and 600 W (Case I).

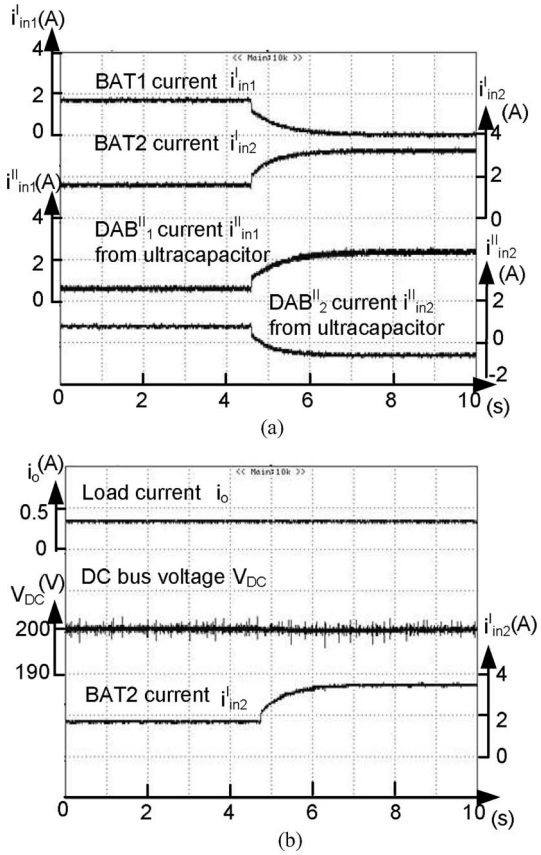

Fig. 17. Experimental result showing the response of the CESS system when output power of BAT1 is made zero. (a) Converter currents. (b) Output voltage (Case II).

Till now, the results for energy management of CESS system are presented to show the capability of the proposed modular power converter structure. In practice, the energy management of a CESS system should be planned by a proper scheduler as shown in [22]. Then, we can avoid circulation of power between battery and ultracapacitor up to a large extent, e.g., ultracapacitor charging can be scheduled when whole CESS system is storing energy and the power converter losses for energy shuffling between battery and ultracapacitor can be avoided. One more situation can be battery replacement. It can be scheduled when current demand from the CESS system is very low. In that

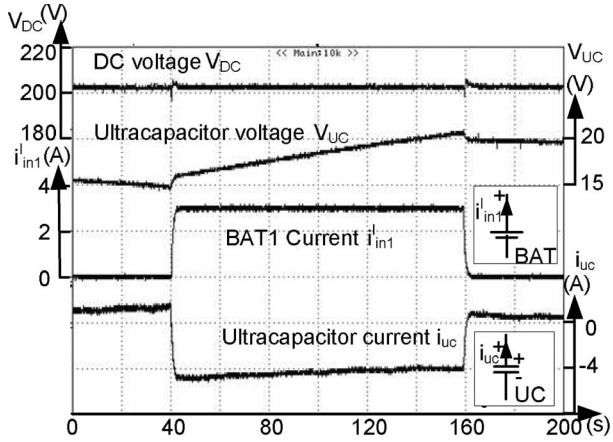

Fig. 18. Experimental result of ultracapacitor charging process (Case III).

case, ultracapacitor itself can support the dc bus during the battery replacement period, and the power flow from other batteries through three power conversion stages can be avoided.

VI. Conclusion

This paper proposes a CESS for microgrid application. This CESS interfaces battery as a high energy density storage, and ultracapacitor as a high power density storage to the dc bus. The dc–dc converter structure is formed using DAB modules whose terminals are connected in series or parallel depending on feasibility. The proposed modular dc–dc converter topology along with its energy management scheme can flexibly share the power between different batteries and ultracapacitor. The scheme is validated using simulation and experiments in this paper.

Appendix

The converters connected to batteries and ultracapacitor are denoted with superscripts I and II, respectively. Hence, their currents and input–output phase shifts are also denoted by same superscripts. As, the dc-link voltage is common for both sides, no such superscript is used to represent it. The subscripts in and o denote the converter input and output variables, respectively. The subscript f signifies that the variable is output of a LPF. The superscript $*$ is used to represent reference values for a particular variable. If there are n converter modules then they can be identified by subscripts 1 to n, respectively.

The voltage controller C_v and current controller C_i shown in Fig. 7 are designed as

$$C_v = K_{cv}\left(1+\frac{1}{sT_{iv}}\right)$$
$$C_i = K_{ci}\left(1+\frac{1}{sT_{ii}}\right). \quad (1)$$

The LPF for the current feedback signals are designed as

$$G_f = \frac{2\pi f_{\rm cf}}{s+2\pi f_{\rm cf}} \quad (2)$$

where f_{cf} is the low-pass filter cutoff frequency. Similarly, the LPF shown in Fig. 8 is in the same format as in (2). All the experimental parameters used in this paper are defined in Table II. Parameters of interleaved DAB converters for interfacing the battery are given here. Same parameters are used for the interleaved converter interfacing the ultracapacitor.

REFERENCES

[1] A. E. Curtright and J. Apt, "The character of power output from utility-scale photovoltaic systems," *IProg. Photovolt: Res. Appl.*, vol. 16, pp. 241–247, 2008.

[2] T. Christen and M. Carlen, "Theory of ragone plots," *J. Power Sources*, vol. 91, no. 2, pp. 210–16, 2000.

[3] M. Glavin, P. Chan, S. Armstrong, and W. Hurley, "A stand-alone photovoltaic supercapacitor battery hybrid energy storage system," in *Proc. 13th Power Electron. Motion Control Conf., 2008 (EPE-PEMC 2008)*, pp. 1688–1695.

[4] Z. Guoju, T. Xisheng, and Q. Zhiping, "Research on battery supercapacitor hybrid storage and its application in microgrid," in *Proc. 2010 Asia-Pacific Power Energy Eng. Conf. (APPEEC)*, pp. 1–4.

[5] R. Dougal, S. Liu, and R. White, "Power and life extension of battery-ultracapacitor hybrids," *IEEE Trans. Compon. Packag. Technol.*, vol. 25, no. 1, pp. 120–131, Mar. 2002.

[6] B. Niemoeller and P. Krein, "Battery-ultracapacitor active parallel interface with indirect control of battery current," in *Proc. Power Energy Conf. Illinois (PECI)*, 2010, pp. 12–19.

[7] G. Guidi, T. Undeland, and Y. Hori, "An optimized converter for battery-supercapacitor interface," in *Proc. IEEE Power Electron. Spec. Conf. (PESC 2007)*, pp. 2976–2981.

[8] W. Li and G. Joos, "A power electronic interface for a battery supercapacitor hybrid energy storage system for wind applications," in *Proc. IEEE Power Electron. Spec. Conf. (PESC 2008)*, pp. 1762–1768.

[9] F. Garcia, A. Ferreira, and J. Pomilio, "Control strategy for battery-ultracapacitor hybrid energy storage system," in *Proc. 24th Annu. IEEE Appl. Power Electron. Conf. Expo. (APEC 2009)*, pp. 826–832.

[10] F. H. Khan and L. M. Tolbert, "Bi-directional power management and fault tolerant feature in a 5-kw multilevel dc-dc converter with modular architecture," *IET Trans. Power Electron.*, vol. 2, pp. 595–604, 2009.

[11] L. Palma and P. N. Enjeti, "A modular fuel cell, modular dc-dc converter concept for high performance and enhanced reliability," *IEEE Trans. Power Electron.*, vol. 24, no. 6, pp. 1437–1443, Jun. 2009.

[12] A. J. Watson, H. Dang, G. Mondal, J. C. Clare, and P. W. Wheeler, "Experimental implementation of a multilevel converter for power system integration," in *Proc. IEEE Energy Convers. Congr. Expo. (ECCE)*, Sep. 2009, pp. 2232–2238.

[13] H. Zhou, T. Bhattacharya, and A. M. Khambadkone, "Composite energy storage system using dynamic energy management in microgrid applications," in *Proc. 2010 Int. Power Electron. Conf.*, Jun.,, pp. 1163–1168.

[14] S. Inoue and H. Akagi, "A bidirectional isolated dc-dc converter as a core circuit of the next-generation medium-voltage power conversion system," *IEEE Trans. Power Electron.*, vol. 22, no. 2, pp. 535–542, Mar. 2007.

[15] H. Zhou and A. M. Khambadkone, "Hybrid modulation for dual-active-bridge bidirectional converter with extended power range for ultracapacitor application," *IEEE Trans. Ind. Appl.*, vol. 45, no. 4, pp. 1434–1442, Jul./Aug. 2009.

[16] R. W. A. A. D. Doncker, D. M. Divan, and M. H. Kheraluwala, "A three-phase soft-switched high-power-density dc/dc converter for high-power applications," *IEEE Trans. Ind. Appl.*, vol. 27, no. 1, pp. 63–73, Jan./Feb. 1991.

[17] W. Chen, R. Xinbo, Y. Hong, and C. K. Tse, "Dc/dc conversion systems consisting of multiple converter modules: Stability, control, and experimental verifications," *IEEE Trans. Power Electron.*, vol. 24, no. 6, pp. 1463–1474, Jul./Aug. 2009.

[18] H. Zhou, A. M. Khambadkone, and X. Kong, "Fast dynamic response in a fuel cell based converter using augmented energy storage," in *Proc. IEEE Power Electron. Spec. Conf. (PESC 2007)*, Sep.,, pp. 1255–1260.

[19] L. Maharjan and E. A. S. Inoue, "State-of-charge (soc)-balancing control of a battery energy storage system based on a cascade pwm converter," *IEEE Trans. Power Electron.*, vol. 24, no. 5, pp. 1628–1636, Jun. 2009.

[20] W. Du, X. Huang, S. Yang, F. Zhang, X. Wu, and Z. Qian, "A novel equalization method with defective-battery-replacing for series-connected lithium battery strings," in *Proc. IEEE Energy Convers. Congr. Expo. (ECCE 2009)*, pp. 1808–1811.

[21] J. Guerrero, J. Vasquez, J. Matas, M. Castilla, and L. de Vicuna, "Control strategy for flexible microgrid based on parallel line-interactive ups systems," *IEEE Trans. Ind. Electron.*, vol. 56, no. 3, pp. 726–736, Mar. 2009.

[22] D. Tran, H. Zhou, and A. M. Khambadkone, "Energy management and dynamic control in composite energy storage system for micro-grid applications," in *Proc. IEEE Ind. Electr. (IECON-2010)*, pp. 1818–1824.

Haihua Zhou (S'07) received the B.E. degree in electrical engineering from the Zhejiang University, China, in 2003 and the M.Sc. degree from the Royal Institute of Technology (KTH), Stockholm, Sweden, in 2005. She is currently working toward the Ph.D. degree at National University of Singapore, Singapore.

Her current research interests include design and control power electronic converter for energy storage applications.

Tanmoy Bhattacharya received the B.E. degree in electrical and electronics engineering from the National Institute of Technology, Tiruchirapalli, India, in 2002, and the M.Sc. (Eng.) and Ph.D. degrees in power electronics from the Indian Institute of Science (IISc), Bangalore, in 2005 and 2009, respectively.

He is currently working as a Research Fellow at National University of Singapore, Singapore. His research interests include hybrid electric vehicles, traction drives, wind, solar hybrid systems, renewable powered micro-grids, etc.

Duong Tran was born in Vietnam. He received the B.E. degree in electrical engineering from Hanoi University of Technology, Vietnam, in 2007. He is currently working toward the Ph.D. degree at National University of Singapore, Singapore.

His research interests include design and control of power electronic converters for dc microgrids and renewable energy systems.

Tuck Sing Terence Siew received the B.E. degree in electrical engineering from the National University of Singapore, Singapore, in 2009.

He is currently a Research Engineer at the National University of Singapore. His research interests include power electronics and real-time digital simulation and testing of hardware systems.

Ashwin M. Khambadkone (SM'04) received the Dr.Ing. degree from the University of Wuppertal, Wuppertal, Germany, in 1995.

He was with the University of Wuppertal; the University of Queensland, Brisbane, Australia; and the Indian Institute of Science, Bangalore, India. In 1998, he joined the National University of Singapore, Singapore, where he is currently an Associate Professor in the Department of Electrical and Computer Engineering. Since April 2010, he has also been the Programme Director at Experimental Power Grid Center (EPGC), Agency for Science, Technology and Research (A*STAR), Singapore. From 1987 to 2001, his research has been concerned with the pulsewidth modulation methods, field-oriented control, parameter identification, and sensorless vector control. His current research interests include distributed-energy-resource networks, renewable energy sources, control of power-electronics-based energy systems, digital control of power factor correction and multilevel inverters.

Dr. Khambadkone was the recipient of the Outstanding Paper Award in 1991 and the Best Paper Award in 2002 from the IEEE TRANSACTIONS ON INDUSTRIAL ELECTRONICS, the Prize Paper Award from the IEEE Industry Applications Society Industrial Power Converter Committee in 2005, and the Outstanding Educator Award in 2008 from the National University of Singapore.